

# Structure of RadB recombinase from a hyperthermophilic archaeon, *Thermococcus kodakaraensis* KOD1: an implication for the formation of a near-7-fold helical assembly

Toshihiko Akiba, Noriyuki Ishii, Naeem Rashid<sup>1</sup>, Masaaki Morikawa<sup>2</sup>,  
Tadayuki Imanaka<sup>1</sup> and Kazuaki Harata\*

Biological Information Research Center, National Institute of Advanced Industrial Science and Technology (AIST), Tsukuba Central 6, 1-1-1 Higashi, Tsukuba, Ibaraki 305-8566, Japan, <sup>1</sup>Department of Synthetic Chemistry and Biological Chemistry, Graduate School of Engineering, Kyoto University, Kyoto 686-8501, Japan and <sup>2</sup>Division of Bioscience, Graduate School of Environmental Earth Science, Hokkaido University, Kita 10 Nishi 5, Sapporo 060-0810, Japan

Received March 1, 2005; Revised and Accepted May 28, 2005

## ABSTRACT

The X-ray crystal structure of RadB from *Thermococcus kodakaraensis* KOD1, an archaeal homologue of the RecA/Rad51 family proteins, have been determined in two crystal forms. The structure represents the core ATPase domain of the RecA/Rad51 proteins. Two independent molecules in the type 1 crystal were roughly related by 7-fold screw symmetry whereas non-crystallographic 2-fold symmetry was observed in the type 2 crystal. The dimer structure in the type 1 crystal is extended to construct a helical assembly, which resembles the filamentous structures reported for other RecA/Rad51 proteins. The molecular interface in the type 1 dimer is formed by facing a basic surface patch of one monomer to an acidic one of the other. The empty ATP binding pocket is located at the interface and barely concealed from the outside similarly to that in the active form of the RecA filament. The model assembly has a positively charged belt on one surface bordering the helical groove suitable for facile binding of DNA. Electron microscopy has revealed that, in the absence of ATP and DNA, RadB forms a filament with a similar diameter to that of the hypothetical assembly, although its helical properties were not confirmed.

## INTRODUCTION

Hyperthermophiles are unique among organisms in that related species grow at remarkably high temperature optima (1). Life at high temperatures poses severe challenges to the stability of DNA, the vital information stores. Spontaneous reactions such as deamination of cytosines and adenines, hydrolytic depurination, and strand breakage are all enhanced at high temperatures, so that organisms need to respond to these challenges by developing robust strategies to ensure the integrity of their chromosomes (2). In particular, powerful DNA repair systems are at work in thermophilic and hyperthermophilic Archaea. For example, *Pyrococcus furiosus* cells are highly resistant to DNA breakage when exposed to temperatures >100°C and are able to reassemble their genomes after extensive fragmentation by gamma irradiation (3,4).

RecA/Rad51 recombinases exist in all three polygenetic domains of life. These proteins, including bacterial RecA, eukaryotic Rad51 and archaeal RadA, are crucial for homologous recombination in repairing double-strand DNA breaks (5,6). In Archaea, there are two groups of proteins, RadA and RadB, which share similarities with the RecA/Rad51 recombinases. The RadA proteins are closer to the Rad51 proteins (~40% amino acid sequence identity) than to the RecA proteins (~20% identity) (7). RadB is smaller than these proteins, consisting of ~220 residues and retaining only the core sequences common to all the RecA/Rad51 family (8,9).

The RadA protein has activities of DNA-dependent ATPase, DNA pairing and strand exchange; for this reason, the protein

\*To whom correspondence should be addressed. Tel: +81 29 861 6194; Fax: +81 29 861 3444; Email: k-harata@aist.go.jp

has been proposed as a counterpart of bacterial RecA and eukaryotic Rad51 proteins in mesophilic and thermophilic Archaea (10,11). However, while the expression of RecA and Rad51 is inducible by UV-irradiation (12,13), RadA is expressed constitutively in *Sulfolobus solfataricus* (7) and in *P. furiosus* (10). The constitutive expression may be necessary for these thermophiles to repair constant DNA damages under severe environments.

The RadB protein has gained less attention than RadA since it was first reported from *Thermococcus kodakaraensis* KOD1 (formerly *Pyrococcus* sp.) (8). Detailed biochemical reports are available only about RadB from *P. furiosus* (PfRadB) (10,14); according to this, it is distinct from RadA. The protein binds dsDNA and ssDNA stronger than RadA, but does not have DNA pairing or strand exchange activity. Its ATPase activity is lower than that of RadA and DNA-independent. Interestingly, PfRadB specifically interacts with the DP1 protein, the catalytic subunit of DNA polymerase D (PolD), to form a complex with it; the complex formation is necessary for PolD to exhibit extensive DNA synthesis activity. Its specific interactions with RadA and Hjc, a Holliday junction resolvase, have been also reported, suggesting some regulatory role on the Holliday junction cleavage activity of Hjc in the recombination process. RadB from *T. kodakaraensis* (TkRadB) shares high amino acid sequence identity with PfRadB (84%), and so it would function similar to PfRadB.

Electron microscopic studies have shown that the RecA/Rad51 family proteins polymerize on DNA to form a helical filament (15–18). Crystal structure of RecA from *Escherichia coli* has demonstrated that the molecules are arranged in a helical polymeric structure in the crystal without DNA (19). A similar helical structure has been generally observed in the crystals of the RecA/Rad51 family proteins including RecA from *Mycobacterium tuberculosis* (20) and *M. smegmatis* (21), Rad51 from *Saccharomyces cerevisiae* (22), and RadA from *Methanococcus voltae* (23). Recently, the formation of oligomeric ring structure has been reported for RadA from *P. furiosus* (24) and human Dmc1 (25).

In this paper, we present the X-ray crystal structure of TkRadB. The structure represents the ATPase domain common in the RecA/Rad51 family, lacking both the N- and the C-terminal domains that have been considered to be responsible for the formation of a ring structure or a helical filament in the RecA/Rad51 proteins. This is the first structural report of an archaeal single domain protein in the RecA/Rad51 family. We have previously reported the crystallization of this protein at a neutral pH condition (formerly called *Pk-REC*); but the crystals were not suitable for X-ray structure analysis because of poor diffraction power and large asymmetric unit that contained >20 molecules (26). We have obtained two new crystal forms; one form enabled us to determine the structure at 2.2 Å resolution.

## MATERIALS AND METHODS

### Crystallization

The TkRadB protein from *T. kodakaraensis* was expressed in *E. coli* and purified as previously reported (27) except that the recloned TkRadB gene was used (28). Two types of crystals (type 1 and type 2) were obtained by the hanging-drop vapour diffusion method. The protein dissolved at 4.9 mg/ml in

50 mM Tris-HCl buffer (pH 8.6) containing 0.2 M NaCl, 0.1 M KCl and 1 mM DTT. A drop solution containing equal volumes of protein and reservoir solutions were equilibrated with the reservoir solution. The type 1 crystal with a rod-like shape was obtained using the reservoir solution containing 0.2 M ammonium sulphate and 30% polyethylene glycol monomethyl ether 2000 at pH 4.6 (0.1 M acetate buffer). The crystal belongs to the orthorhombic space group  $P2_12_12_1$  with cell dimensions  $a = 46.01$ ,  $b = 82.47$  and  $c = 111.94$  Å. The asymmetric unit contained two independent molecules ( $V_m = 2.2$ ). The type 2 crystal with an octahedral shape was prepared using the reservoir solution containing 20% PEG6000 and 2.0 M lithium sulphate at pH 4.6 (50 mM citrate buffer). The type 2 crystal was of the same space group and also contained two independent molecules in the asymmetric unit ( $V_m = 2.4$ ). The cell dimensions were  $a = 59.73$ ,  $b = 82.89$  and  $c = 96.79$  Å.

### Structure determination and refinement

The initial structure of TkRadB was obtained by the MIR method using the type 1 crystal. The native data were collected to 2.4 Å resolution on a Bruker smart6000 diffractometer equipped with MacScience MH06 rotating anode generator (50 kV, 90 mA, focal spot size 0.3 mm) and Osmic Max-Flux confocal optics. Three heavy atom derivative crystals were used for the phase determination. The collected data were indexed and integrated with SMART and SAINT+ (Bruker AXS, Madison, USA). Calculation of experimental phases at 2.9 Å resolution followed by the density modification was carried out using the program autoSHARP (29) along with programs in the CCP4 suite (30). Structure models were built with TURBO-FRODO (31) and refined at 2.6 Å resolution with X-PLOR (32).

Intensity data of the native type 2 crystal was collected to 2.1 Å resolution under a cryogenic condition (100 K) at the BL6A beam line of the Photon Factory in KEK, Tsukuba, using an ADSC Quantum-4R CCD detector, and processed with HKL2000 (33). The structure was solved by the molecular replacement method using CNS (34) and refined at 2.2 Å resolution in the same way as the type 1 crystal structure. The data collection and refinement statistics are summarized in Table 1 along with those of the type 1 crystal. Coordinates and diffraction data of the type 1 and type 2 crystal structures have been deposited in the Protein Data Bank (PDB) with ID codes of 2CVF and 2CVH, respectively.

Comparison and superposition of molecular structures were performed with TOPP (35) and LSQKAB (36) in the CCP4 suite. The molecular figures were prepared with Molscript (37) and PyMol (<http://www.pymol.org>). Electrostatic potentials were calculated with DelPhi (38) and the surface models were prepared with Insight II (Accelrys Inc., San Diego, USA).

### Electron microscopy

A TkRadB solution used for the crystallization was diluted with the buffer containing 20 mM Tris-HCl (pH 7.6), 15 mM  $MgCl_2$  and 2 mM DTT to a final protein concentration of 50 µg/ml, and then incubated at 60°C for 15 min or 90°C for 15 min. An aliquot was applied to a glow-discharged grid covered with carbon support film and negatively stained with 1% uranyl acetate for 1 min. Specimens were examined in

**Table 1.** Crystallographic data and refinement statistics

	Type 1 crystal Heavy atom derivatives HgCl <sub>2</sub>		K <sub>2</sub> PtCl <sub>4</sub>	KAu(CN) <sub>2</sub>	Native	Type 2 crystal Native
Space group	P2 <sub>1</sub> 2 <sub>1</sub> 2 <sub>1</sub>					P2 <sub>1</sub> 2 <sub>1</sub> 2 <sub>1</sub>
Cell constants						
<i>a</i> (Å)					46.01	59.73
<i>b</i> (Å)					82.47	82.89
<i>c</i> (Å)					111.94	96.79
Data collection statistics <sup>a</sup>						
Resolution range (Å)	24.7–2.50 (2.64–2.50)	24.4–2.90 (3.06–2.90)	24.9–2.60 (2.74–2.60)	24.7–2.40 (2.53–2.40)	29.88–2.03 (2.14–2.03)	
Observed reflections	111 203 (6287)	61 888 (8025)	83 401 (8495)	167 114 (13 021)	224 019 (29 346)	
Unique reflections	13 990 (1566)	9502 (1282)	13 094 (1590)	16 828 (2249)	31 513 (4369)	
Multiplicity	7.6 (3.6)	6.4 (6.1)	6.2 (4.9)	9.8 (5.6)	7.1 (6.7)	
Completeness (%)	98.2 (93.1)	99.2 (98.6)	98.8 (94.6)	99.5 (98.7)	99.8 (99.6)	
Mean <i>I</i> /σ( <i>I</i> )	5.7 (2.9)	6.2 (3.4)	5.6 (2.3)	7.2 (2.7)	26 (10.5)	
<i>R</i> <sub>merge</sub> (%)	11.0 (24.4)	10.9 (21.6)	12.3 (31.4)	8.5 (24.4)	4.8 (17.0)	
Phasing statistics						
Phasing power (centric/acentric)	1.22/1.03	0.55/0.60	1.21/0.90			
(anomalous)	0.94	0.48	0.51			
Figure of merit (centric/acentric)	0.57/0.60					
Refinement statistics						
Resolution range				6.0–2.6	6.0–2.2	
No. of reflections				11 912	22 756	
Completeness (%)				95.2	96.5	
Cutoff criteria				<i>F</i> <sub>o</sub> >2σ ( <i>F</i> )	<i>F</i> <sub>o</sub> >2σ ( <i>F</i> )	
No. of protein molecules				2	2	
No. of water molecules <sup>b</sup>				189	297	
<i>R</i>				0.235	0.193	
<i>R</i> <sub>free</sub>				0.304	0.253	
RMSD						
bond lengths				0.008	0.011	
bond angles				1.78	1.68	

<sup>a</sup>Values in parentheses are of the outermost resolution shell.

<sup>b</sup>Water molecules were placed at high peaks (>2.5 s) in the *F*<sub>o</sub>–*F*<sub>c</sub> difference Fourier map and, in the following refinement, those with large B factors (>60 Å<sup>2</sup>) were removed.

a Philips Tecnai 20F electron microscope operated at 120 kV and images were recorded at a magnification of 50 000 on Kodak electron image films (SO163) using a low dose system.

## RESULTS

### Molecular structure

The structures of the TkRadB monomer obtained from two crystal forms were very similar. A ribbon model of the type 2 crystal structure is presented in Figure 1. TkRadB consists of compactly packed secondary structural elements, seven helices and nine β-strands. The twisted sheet composed of nine β-strands winds around the core helix H2. The three helices, H5, H6 and H7, are located on the outer surface of the sheet. The two helices, H3 and H4, form a bundle structure with H2. In spite of rather low similarity in the amino acid sequence, the main chain fold of TkRadB closely resembles that of the RecA/Rad51 ATPase domain structures reported so far, which include the crystal structures of *E.coli* RecA (EcRecA) (19), human Rad51 (HsRad51) (39), human Dmc1 (HsDmc1) (25) and *P.furiosus* RadA (PfRadA) (24). Among these four homologous proteins, PfRadA shares the highest sequence identity (35%) with TkRadB (Figure 2), having an RMSD of 1.23 Å for 166 Cα atoms as compared with the structure in Figure 1. The other three, EcRecA, HsRad51 and HsDmc1, have 30, 30 and 27% sequence identity, respectively, exhibiting RMSD values of 1.52, 1.32 and

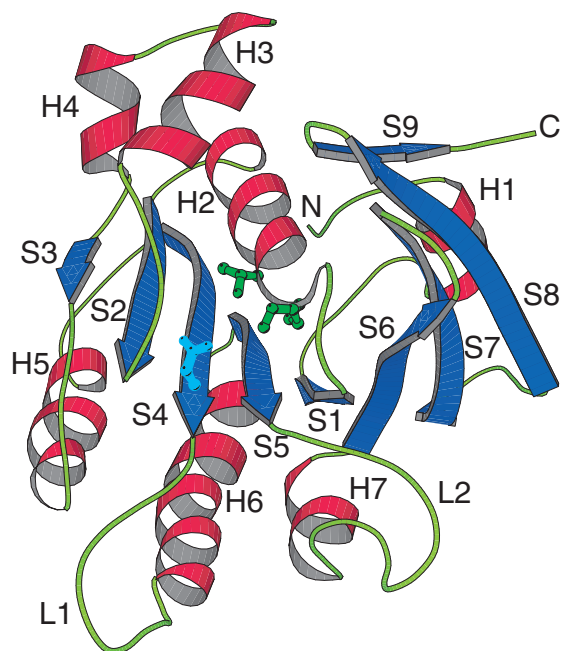


**Figure 1.** Ribbon representation of TkRadB. α-Helices and β-strands are denoted by H1–H7 and S1–S9, respectively, and the N- and C-terminals by N and C, respectively. The L1 and L2 loops are also labelled. Side-chains of Lys-33, Thr-34 and Asp-112 are presented as ball-and-stick models to show the location of the ATP binding site; the first two of the Walker A motif are in green and the last one of the Walker B motif in cyan.

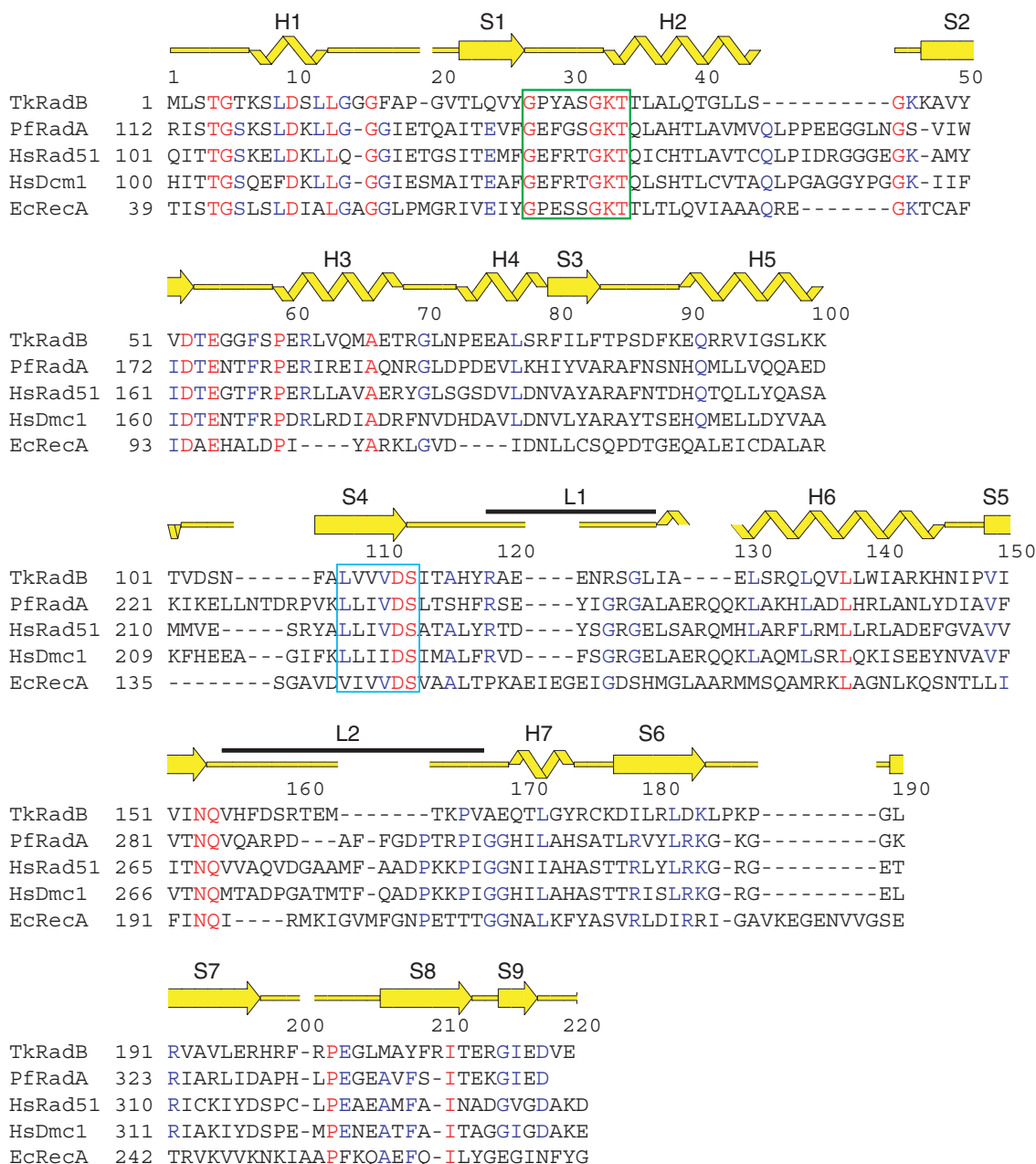


**Figure 2.** Sequence alignment of TkradB with homologous proteins, *Pyrococcus furiosus* RadA (PfradA), human Rad51 (HsRad51), human Dcm1 (HsDcm1) and *E. coli* RecA (EcRecA). The Walker A and B motifs are indicated by green and cyan boxes, respectively. The secondary structure elements of TkradB are shown above the alignment with the same notation as in Figure 1. Similarly indicated are the L1 and L2 loop regions.

1.27 Å for 159, 164 and 173 C $\alpha$  atoms, respectively. The present structure demonstrates that RadB represents the core domain of the RecA/Rad51 family proteins and that the deletion of neither the N-terminal domain of PfradA nor the C-terminal domain of EcRecA significantly affects the basic fold of the core domain. It seems to explain the fact that RadB possesses ATPase and DNA binding activities, which are commonly observed in the RecA/Rad51 family proteins. The Walker A and B motifs (40), the ATP binding sequence motifs highly conserved in these proteins, are located at the N-terminal side of the helix H2 and at the C-terminal side of the strand S4, respectively (Figures 1 and 2). The presumed DNA binding loops, L1 and L2, which are between

S4 and H6, and between S5 and H7, respectively, are poorly ordered as indicated by weak electron densities, suggesting that they are highly flexible or in multiple conformations.

### Dimeric structure

Both the crystals contain two molecules in the asymmetric unit. In the type 1 crystal, two monomers in the asymmetric unit are not related by a simple non-crystallographic symmetry (Figure 3a), but they can be assumed as a part of a near-7-fold helix as discussed later. The two monomers are tightly bound; an extensive surface area containing >15 residues in each

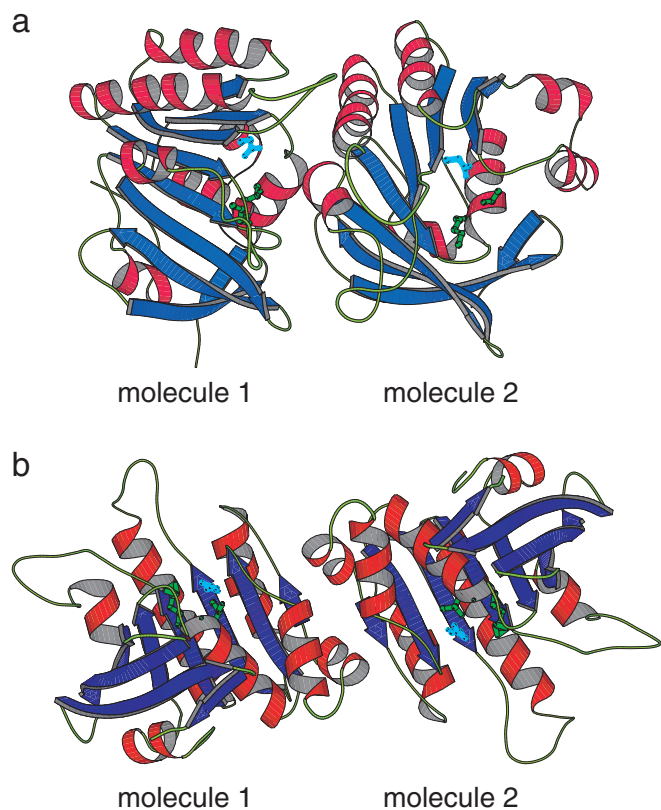


**Figure 3.** Structures of the asymmetric unit of the type 1 crystal (a) and the type 2 crystal (b). Side-chains of Lys-33, Thr-34 and Asp-112 in each monomer are presented as ball-and-stick models as in Figure 1. In (b), the non-crystallographic 2-fold rotation axis is perpendicular to the figure plane.

monomer is involved in the direct contact between them. The total reduction of solvent accessible area by dimerization is estimated to be  $2951 \text{ \AA}^2$ , which corresponds to 28.2% of the total surface area of the monomer and which is larger than the corresponding value of  $2890 \text{ \AA}^2$  (19.4%) in the EcRecA polymer (19). Figure 4 depicts characteristic charge distributions on the molecular surface of the TkRadB monomer: a positively charged patch (Figure 4a) and a negatively charged one (Figure 4b). The interaction surface of molecule 1 includes the negatively charged patch, which contains no basic amino acid but which is rich in acidic amino acids including Glu-54, Asp-87, Glu-122, Asp-158 and Glu-162. The positively charged patch is used in the interface of molecule 2; there are one lysine and seven arginine residues (Lys-177, Arg-124, Arg-133, Arg-160, Arg-175, Arg-197, Arg-199 and Arg-201), but one glutamic acid, Glu-169, is also located there. There are 15 polar contacts containing three salt linkages between the two monomers. The monomer–monomer interface thus formed between the oppositely charged patches indicates that the electrostatic interaction provides a major binding force for dimerization.

In the type 2 crystal, two monomers are related by non-crystallographic 2-fold symmetry as shown in Figure 3b as viewed from the symmetry axis. The positively charged patches of both the two monomers face the same direction along the symmetry axis. The monomers contact each other at

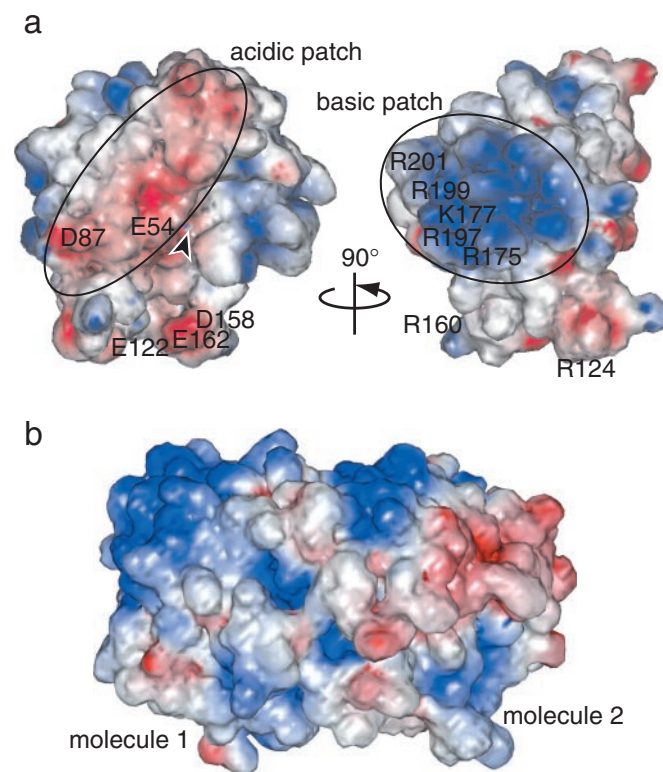


**Figure 4.** Surface electrostatic potentials of TkRadB in the type 1 crystal. Acidic and basic regions are coloured red and blue, respectively. (a) Two orthogonal views of the monomer (molecule 1 in Figure 3a). Positions of the residues involved in the intermolecular interface are labelled by the one-letter amino acid code and the sequence number (see text); the arrowhead indicates the ATP binding site. (b) Dimer in the asymmetric unit oriented as in Figure 3a.

the sides of two helices H3 and H4, where acidic amino acid residues, Asp-52, Glu-60, Glu-67 and Glu-74 participate in intermolecular hydrogen-bonding through their side-chains.

#### ATP binding site

Two ATP binding sites in the type 2 crystal dimer are each equivalently located on the surface and exposed to solvent (Figure 3b). The structures of both the sites are very similar to those in the RecA/Rad51 family proteins. In contrast, the binding sites in the type 1 dimer are not in an equivalent environment: the one in molecule 2 is open to solvent but the other one in molecule 1 faces the molecular interface of the dimer, lying in a deep crevice between two monomers (Figures 3a and 4a). Their structures are also slightly different: the latter is similar to those in the type 2 structure, but the former is slightly different from them as will be described later.

In the type 1 crystal structure, it would be of interest if binding of the nucleotide to the catalytic site in the molecular interface affects the interaction between monomers; but, unfortunately, the TkRadB crystals have been obtained only in the absence of nucleotides. Introduction of ADP or non-hydrolyzable ATP analogues into the crystals by post-soaking was unsuccessful: the electron-density map of the crystal immersed in the solution containing ADP or a slowly hydrolyzable ATP analogue, ATP $\gamma$ S, showed no electron densities

associated with the ligand molecule. The co-crystallization with the analogues was also unsuccessful since the addition of the analogues to the protein solution caused amorphous precipitation before adding crystallization reagents. Accordingly, the structure of the MvRadA protein in complex with AMP-PNP (23), a non-hydrolyzable ATP analogue, was employed to place the analogue in the ATP binding site at the interface by superposition. MvRadA has 31.3% sequence identity with TkRadB. The MvRadA protein structure was superposed onto molecule 1 of the type 1 dimer with an RMSD of 1.58 for 164 C $\alpha$  atoms (Figure 5a). The superposition seems good and, as a result, the AMP-PNP molecule is placed reasonably well in the ATP binding site of TkRadB molecule 1 except for obvious conflicts at the side-chains of Lys-33 of molecule 1 and Arg-197 of molecule 2 (Figure 5b). The former conflicts with the  $\beta$ -phosphate of the adapted AMP-PNP and the latter with its sugar moiety. However, since there is ample room around these side-chains, they can readily change their conformation to dodge the ligand without posing other conflicts. In the present structure, these side-chains extend into the unoccupied intermolecular cavity, making water-mediated hydrogen bonds to each opposite molecule. Apart from these side-chains, the adapted ligand conflicts with neither of the protein molecules. It is noteworthy that the adenine ring of the placed nucleotide analogue is sandwiched by Arg-61 of molecule 1 and Pro-202 of molecule 2 similarly to that in the MvRadA filament, where Arg-158 and Pro-307 of that protein correspond to these two residues, respectively (23). This proline is widely conserved in the RecA/Rad51/RadA proteins and the RadB proteins from *Pyrococcus* species but, interestingly, not so in RadBs from other archaeal bacteria. On the other hand, that arginine is common to eukaryotic Rad51/Dmc1 and archaeal RadA/RadB proteins but are replaced by tyrosine in bacterial RecA. Judged from these results, nucleotide-bound TkRadB molecules would be able to aggregate in the same way as the present structure. In such a case, the bound nucleotide would be trapped in the binding site because the opening of the site to the solvent is too small as realized in Figure 5b.

### Helical assembly model

The TkRadB molecules are arranged along the crystallographic 2-fold screw axes in both the two types of crystals. Therefore, the crystal packing does not reflect the fibrous structure as reported for many of the RecA/Rad51 protein crystals. However, a careful inspection of the type 1 crystal structure has revealed that the two independent molecules in the asymmetric unit are roughly related by 7-fold screw symmetry. By applying an appropriate transformation on the matrix relating the two molecules, it has been demonstrated that the two molecules are on a right-handed helical track with a pitch of 113.4 Å containing 6.57 monomer units/turn. Thereby, iterative application of the matrix on the TkRadB monomer coordinates produces a helical structure (Figure 6). The helix pitch of 113.4 Å falls in the range of reported pitches of the RecA/Rad51/RadA helical filaments in the crystals (67–130 Å) (19–23,41,42). Since the axes of these filaments coincide with the P6<sub>1</sub> axis in their crystals, they all contain 6 monomers/turn. The RecA/Rad51/RadA helical filaments observed by electron microscopy, which are not bound to

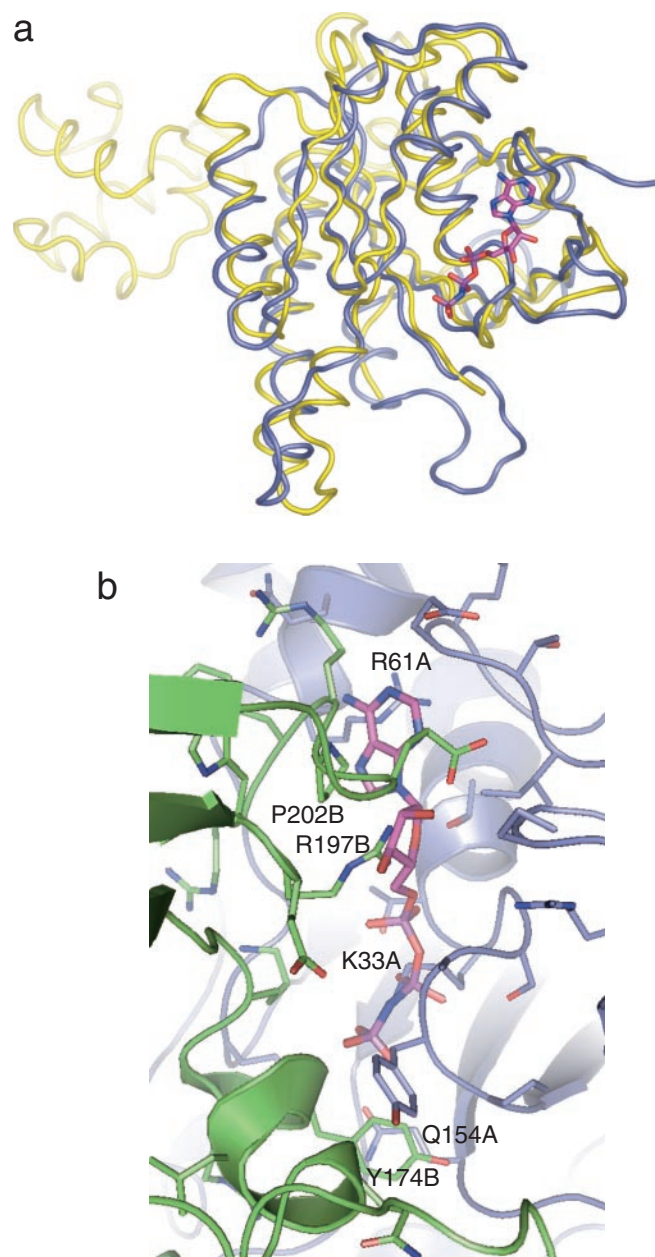


**Figure 5.** ATP-binding site of TkRadB with an AMP-PNP molecule adapted by superposition. (a) Superposition of the AMP-PNP-bound MvRadA molecule (PDB ID:1T4G; yellow) to the TkRadB molecule (molecule 1 of the type 1 dimer; blue). Two protein molecules are presented as C $\alpha$ -tracing tube models. (b) The ATP-binding site of the TkRadB type 1 structure with the AMP-PNP molecule. The TkRadB monomers are in a ribbon presentation; molecule 1 is in blue and molecule 2 in green. Side-chains of amino acid residues within 6 Å from the AMP-PNP molecule are presented as sticks. Several residues of interest are labelled by each one-letter code, sequence number and chain ID (see text). The AMP-PNP molecule is presented as a magenta stick model in both figures.

the crystal symmetry, have 6.1–6.6 monomers/turn helices with pitches of 76–100 Å (16–18). Thus, the helix parameters of the TkRadB assembly model are compatible with those of the documented RecA/Rad51/RadA filaments.

A characteristic charge distribution is observed on the surface of this right-handed helix model of TkRadB (Figure 7).

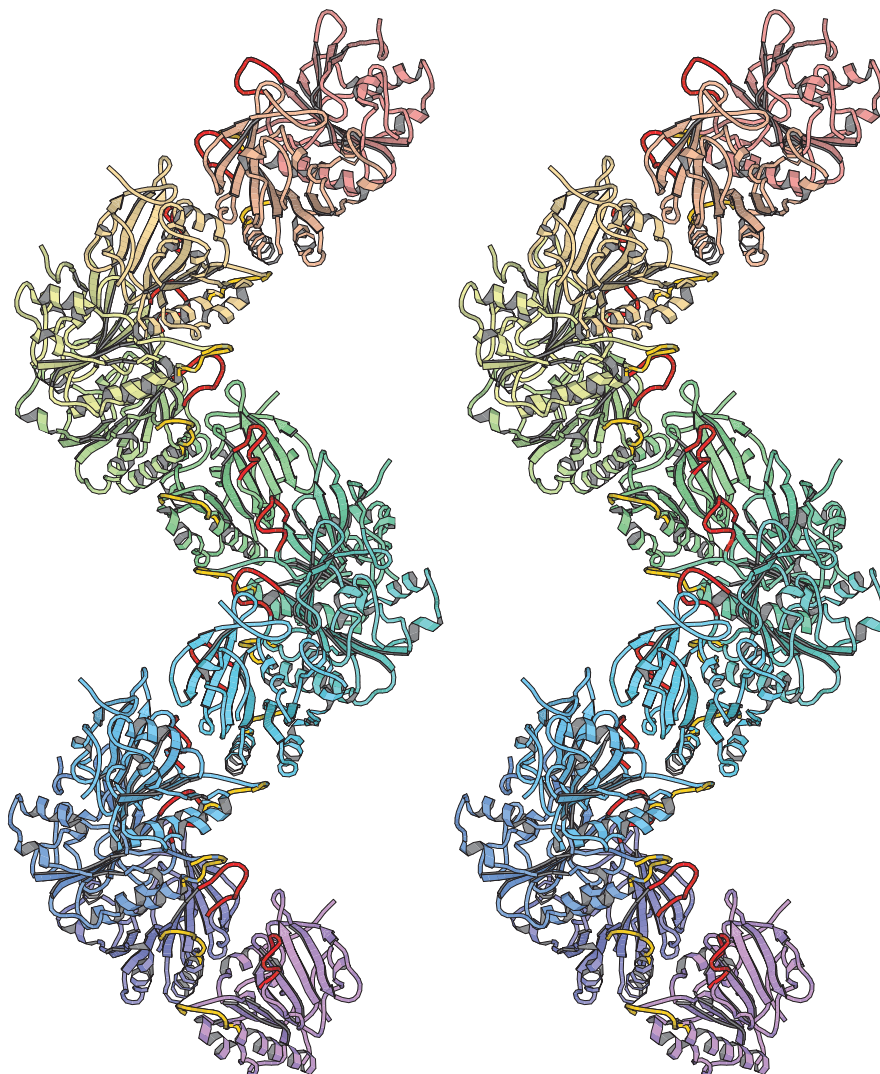


**Figure 6.** Stereo-drawings of the helical assembly of TkRadB in ribbon representation. Each TkRadB monomers are in different colours. Yellow and red segments in each monomer indicate the L1 and L2 loops, respectively.

Two loop regions, L1 and L2, point towards the centre of the helix (Figure 6), making the inner surface rather acidic with Glu-121 and Glu-122 in the L1 loop and Asp-158 and Glu-162 in the L2 loop. The TkRadB helix model has a large and open helical groove. The ATP binding site opens in the positively charged deep pocket on one surface bordering of this groove. On the other side of the groove is a positively charged helical belt, which is clearly distinguished from the inner surface of the helix having slightly acidic nature.

### Filament formation

Inspired by the helical assembly model, we have examined the TkRadB protein in solution under the electron microscope. An electron micrograph of TkRadB shows the formation of fibrous assemblies in the absence of DNA and ATP (Figure 8). The diameter of the observed filament was  $\sim 100$  Å, which is in good agreement with that of the hypothetical structure described earlier. The filament displays seemingly periodic variations in diameter partially along the length (indicated

by arrowheads in Figure 8), which implies its helical nature. The filaments were dominantly observed after the incubation at  $60^\circ\text{C}$  but not at  $90^\circ\text{C}$  or at room temperature. The observation indicates that they are not products of non-physiological denaturation like amyloid fibrils, but of a certain physiological process. The appearance of the filaments is clearly different from the typical twisted-tape appearance of amyloid fibrils. Image analysis of the electron micrographs was attempted to confirm helical arrangement of the molecules in the filaments but not successful: computed diffraction patterns of the filament images did not show layer-lines typical of helical objects. The observation of TkRadB in the presence of adenine nucleotides was also attempted, but hampered by extensive aggregation of the protein.

### Asymmetry of the monomers in the type 1 dimer

A possibility of the helical filament formation presented in the previous section poses a question: why the protein crystallized in a dimeric form instead of polymerizing further in the type 1

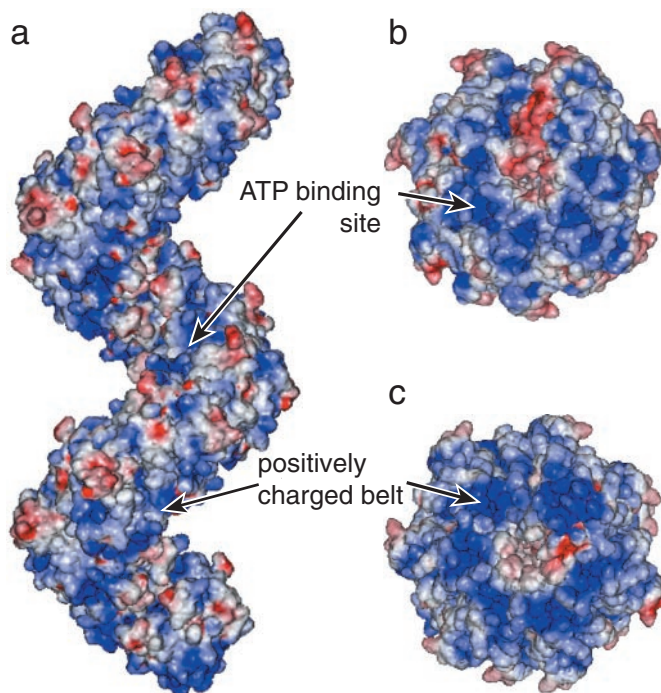


**Figure 7.** Surface electrostatic potentials of the helical assembly of TkRadB. The helix model in surface representation is viewed perpendicular to the helix axis (a), from the top of the assembly (b) and from the bottom (c). Acidic and basic regions are coloured red and blue, respectively. The locations of the ATP-binding site and the positively charged belt (see text) are indicated by arrows.

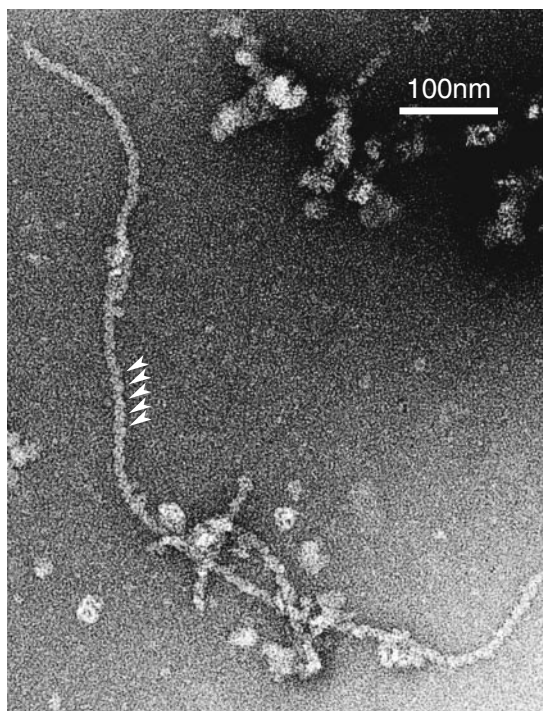


**Figure 8.** Electron micrograph of the TkRadB filament which was formed during the incubation at 60°C for 15 min. White arrowheads indicate periodic changes in the filament diameter. The scale bar represents 100 nm.

crystallization conditions. The first step of polymerization is most likely to be dimerization and the dimerization could cause changes in the monomer structures, making further association difficult. To examine equivalence between two monomers in the asymmetric unit, they were compared by superposition and the results were compared between the two crystal forms. Two independent molecules in the type 1 crystal are superimposed with an RMSD of 1.36 Å for 158 C $\alpha$  atoms, whereas those in the type 2 crystal with an RMSD of 0.66 Å for 200 C $\alpha$  atoms. In the comparison of each distance between the corresponding C $\alpha$  atoms in the superimposed structures (Figure 9a), exceptionally large deviations (>5 Å) were observed for the type 1 crystal in limited residues in addition to those within or near the highly mobile L1 and L2 loops. They are Ser-31, Gly-56, Phe-57, Pro-188 and Gly-189. These residues are located within or near the interface region (Figure 9b). In molecule 1, Phe-57 and Pro-188 are involved in direct hydrogen bonding to molecule 2 along with His-117 and Tyr-118 in the L1 loop. Ser-31 of molecule 1, the fifth residue of the Walker A motif, should interact with phosphate group of the bound nucleotide, but the C $\alpha$  atom of Ser-31 of molecule 2 is deviated to a position directly conflicting with the  $\beta$ -phosphate of the AMP-PNP molecule adapted to molecule 1 by the superposition. This conformation could impair proper binding of the nucleotide. Thus, another interface region around the ATP binding site of molecule 2 is apparently different from that of molecule 1. However, we are not sure about its impotency for molecular association. When molecules 1 and 2 are swapped by mutual superposition to examine the compatibility of the new interface, nine apparent atomic conflicts are counted at least; but they are not inter-main-chain conflicts, and so they can be resolved by conformation changes of the side-chains.

## DISCUSSION

### Molecular interface and surface charge distribution

TkRadB was crystallized in two crystal forms in relatively low pH conditions. The protein is supposed to be highly charged in these conditions or at ordinary neutral pH because it has a rather high pI of 9.35 estimated from the amino acid sequence. The crystal structure obtained reveals a characteristic charge distribution on the molecular surface: two distinctive patches, positively charged and negatively charged ones, are noticed on the surface. They form the interface of the dimer in the type 1 crystal. The type 1 crystal was grown in the lower salt concentration (0.2 M ammonium sulphate in the reservoir solution) whereas the type 2 crystal was obtained in the presence of 2 M LiCl in the reservoir solution. The considerably low solubility of TkRadB in a solution with low ionic strength may be ascribed to strong ionic interaction between these patches, which would lead to extensive aggregation of the molecules. The helical assembly was not observed in the solution environment of high ionic strength. These observations agree with the structural implication that an appropriate electrostatic interaction is crucial for molecular association that could lead to helical assembly. A similar form of electrostatic interaction by the complementarily charged surfaces has been pointed out for the interfaces in the bacterial RecA proteins (42).

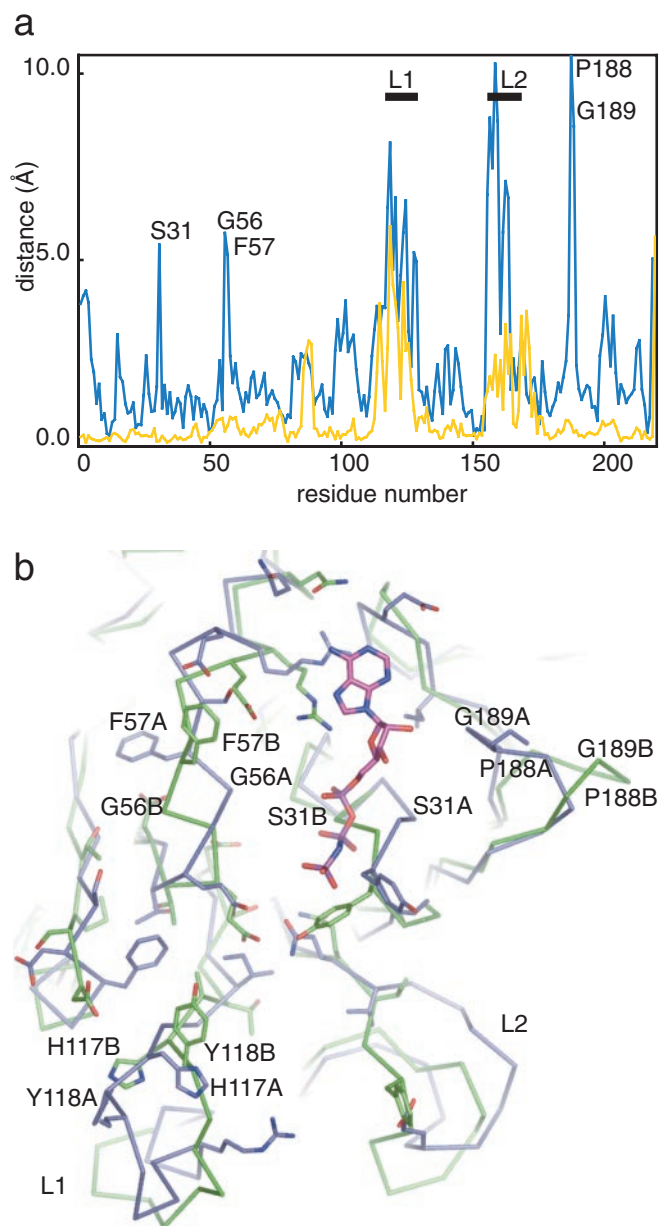


**Figure 9.** Structural comparison of monomers in the type 1 dimer. (a) Comparison of structural differences between monomers in the type 1 and type 2 crystal structures. Distances between the C $\alpha$  atoms of the corresponding amino acid residues in two monomers are plotted against the residue number for the two structures (blue for type 1 and yellow for type 2). The L1 and L2 loop regions and the residues showing exceptionally large deviations are labelled. (b) Superposition of two monomers in the type 1 dimer. Molecule 1 and 2 are presented in blue and green C $\alpha$ -traces, respectively. Side-chains of amino acid residues within 4 Å from the adjacent monomer are presented as sticks. The AMP-PNP molecule in a magenta stick model is placed in the ATP-binding site of molecule 1 as in Figure 5. The L1 and L2 loops and several residues of interest are labelled (see text).

### Helical assembly model and the ATP binding site

Both the type 1 and 2 crystals contain two independent molecules in the asymmetric unit, which are related by near-7-fold screw symmetry in type 1 and by 2-fold symmetry in type 2. The former structure suggests formation of a helical

assembly of the protein in solution. The helical assembly model is based on the interface in the asymmetric unit and, therefore, independent of the crystallographic symmetry of the crystal. Probably for this reason, the number of monomer units per turn of the model (6.57) is similar to those obtained from the RadA/Rad51 filament images by electron microscopy (6.1–6.6).

Two forms of the RecA/Rad51 filaments are documented: an extended active form and a compressed inactive form. The extended filament is formed on DNA in the presence of ATP or an ATP analogue, having a helical pitch of 90–130 Å; the compressed form is obtained without DNA or ATP, having a pitch of 65–85 Å (16,18). Most of filament structures based on the crystal structures of the RecA/Rad51 homologues have pitches of 67–83 Å and are, therefore, considered as a compressed form (19–21,41,42). The helix pitch of the present assembly model of TkRadB is 113.4 Å, which should label the model as in the extended conformation.

We employed the crystal structure of MvRadA in complex with AMP-PNP (23) to examine adaptability of the analogue to the buried ATP binding site in the type 1 structure. It is considered as the first high-resolution structure of the extended conformation, providing a filament with a pitch of 106.7 Å. The MvRadA structure is markedly different in the interfaces between adjacent core domains from the crystal structures of PfRadA and EcRecA: the ATP cap (Asp-302–Asp-308) and the C-terminal L2 elbow regions of the adjacent monomer are much closer to the ATP binding site in MvRadA than in PfRadA and EcRecA; namely, the ATP binding site of MvRadA looks ‘closed’ and the others look ‘open’. In addition, the subunit interfaces of the MvRadA structure are similar to that of the active RecA filament model based on electron microscopy. Figure 5b depicts that the interface between the TkRadB monomers in the type 1 structure resembles the ‘closed’ conformation of the MvRadA structure: the putative ATP binding cavity is covered by the S7–S8 loop corresponding to the ATP cap of MvRadA and the C-terminal of H7 helix downstream of the L2 loop of the adjacent monomer. Close association between the catalytic site and the L2 loop has been proposed to couple ATP hydrolysis with manipulation of DNA. Particularly interesting in MvRadA is an intermolecular contact between Gln-257 at the upstream of the L2 loop and His-280 at the downstream of L2 of the neighbouring molecule; it is conserved as a Gln-154–Tyr-174 pair in TkRadB and a Gln-194–Phe-217 pair in the microscopy-derived model of EcRecA. The similarity in association is also clearly indicated by superposition: the type 1 dimer of TkRadB is superimposed to the two P6<sub>1</sub>-symmetry-related adjacent monomers of MvRadA with an RMSD of 1.8 Å for 310 C $\alpha$  atoms. Likewise, the MvRadA filament with AMP-PNP resembles the model filament in the axial region; particularly, the L1 and L2 loops extend towards the helix axis and are arranged in a very similar way in both filaments (Figure 6). An agreement about the helix pitch between two filaments is also natural. Consequently, the TkRadB filament model would be of an extended active conformation characterized by a direct contact of the ATP binding site with the adjacent monomer in spite that the protein is free of DNA and ATP.

The ‘closed’ conformation of the ATP binding site has also been observed in the crystal structure of Rad51 from *S.cerevisiae* (ScRad51) (22). Interestingly, in spite that the

crystal was grown in the presence of DNA and ATP $\gamma$ S, neither of them has been visualized; in the nucleotide-binding site, only the putative phosphate site seems to be occupied with a sulphate ion. The vacancy of the binding site has been ascribed to an escape of the hydrolyzed analogue during a long period of crystallization process, suggesting release of the hydrolyzed product may not affect the structure. The ScRad51 filament structure is also unique in having an asymmetric dimer unit, which would account for double affinities to ATP observed in EcRecA (43). This asymmetry arises from differences in orientation of the N-terminal domain and, therefore, it is totally different from the one we have observed in the type 1 dimer.

For the PfRadB protein, filament formation has been observed under the electron microscope (10). In the absence of DNA and ATP $\gamma$ S, the protein forms seemingly helical filaments  $\sim$ 200 Å in diameter as judged from Figure 6A of the report. In the absence of DNA but with ATP $\gamma$ S, it also forms filaments, but they look different from the previous ones: they are smooth and  $\sim$ 100 Å thick, forming extensive bundles. On the other hand, the PfRadA protein forms rings in both these conditions. We have observed the filaments of TkRadB in the absence of ATP and DNA (Figure 8), which measure  $\sim$ 100 Å in diameter with barely periodic variations in thickness. Puzzlingly, they look more like the PfRadB filaments formed in the presence of ATP $\gamma$ S than those without ATP $\gamma$ S. Computed diffraction patterns of filament images would have helped the comparison, but such data have not been provided for the PfRadB filaments. As described earlier, similar attempts for the TkRadB filaments were not successful either. The lack of this kind of quantitative image data also makes it difficult to identify the TkRadB helix model based on the type 1 crystal with the microscopically observed RadB filaments. Notwithstanding, we think it is likely that the TkRadB model filament corresponds to the 100-Å thick filament observed under the electron microscope. According to the model, the RadB protein may form a similar filament regardless of ATP. The doubly thicker PfRadB filament formed without the ATP analogue is unusual; perhaps, it may be formed by supercoiling of a 100-Å thick protofilament or twisting the two protofilaments because no RecA/Rad51 protein filament has been reported with such a large diameter. The TkRadB model filament seems to be prone to deformation during negative staining because of its small diameter and large open groove. Altogether, the RadB apoprotein or its ATP-bound form may polymerize in an extended active form. The ATP-bound protein might be favoured in polymerization since the ligand molecule that fills the active site cavity in the interface is expected to increase the number of interactions between monomers.

As the TkRadB structure represents only the core domain of the RecA/Rad51 proteins, the filament formation of RadB would suggest that polymerization can be an intrinsic capability of the core domain. Nevertheless, the N- and C-terminal domains, both of which are missing in TkRadB, are involved in molecular association in the RecA/Rad51 filaments or rings; moreover, they are shown to be necessary for polymerization in some cases (44,45). TkRadB also lacks the oligomerization motif commonly observed in other RecA/Rad51 filament structures (19,23,24). This conserved motif is a short  $\beta$ -strand in the flexible linker region between the N-terminal and the core ATPase domains of these proteins. It forms an intermolecular

sheet with a  $\beta$ -strand of the adjacent ATPase core domain, which corresponds to the S3 strand of TkRadB. The S3 strand is not involved in the intermolecular interaction in the type 1 structure, residing at the periphery of the model helix, while it is used to bind a 2-fold symmetric dimer in the type 2 crystal (Figure 3b). Owing to binding through the polymerization motif and the N- and C-domains, the RecA/Rad51 homologues other than RadB can enjoy a freedom of the core domain movement even in filament forms; but the RadB protein in the filament may have a very small margin for movement.

The dimer structure in the type 1 crystal shows that the ATP binding site of molecule 1 seems to be in a 'closed' conformation. Namely, it is buried in the deep crevice formed between the two molecules and hardly accessible by the substrate from the outside while it may or may not hold the substrate in place. This implies dimerization of the protein may stop binding or turnover of the substrate to reduce the ATPase activity, unless hydrolysis of ATP induces structural changes to open the binding site. The ATPase activity of PfRadB is lower than that of PfRadA and stops at a protein:ATP ratio of about unity, suggesting lack of the enzymatic turnover (10). According to our model, the observation can be explained by assuming that the ATP binding facilitates molecular association and that the hydrolysis does not open the binding site. On the other hand, conformational changes following ATP binding has been suggested from microscopic observations of filaments without DNA and also from results of the gel shift assay (10). The binding patterns of PfRadB to ssDNA with and without ATP are different: the size of protein-nucleic acid complex produced increases as the amount of applied PfRadB in the absence of ATP but it is constant in the presence of ATP. It does not contradict our model because possible changes are not necessarily limited in or near the ATP binding site and because the putative DNA binding site does not seem to be shared by the ATP binding site. Conversely, very small changes around the ATP binding might be amplified allosterically by a leverage mechanism. Escape of the product from the 'closed' ATP binding site has been pointed out in the ScRad51 filament (22); however, it may take much longer time in the TkRadB dimer because the opening of the site in the ScRad51 filament looks  $>4$  Å wider than that in the present structure.

### DNA binding and related functions

The TkRadB helix has a positively charged belt on one side of the helical groove. The belt may provide a suitable binding site for DNA (ssDNA/dsDNA) along the helix. High pI value of TkRadB should favour the electrostatic binding of DNA. Little difference between preferences of PfRadB for dsDNA and ssDNA (10) implies that both types of DNA might share this putative DNA binding site. The helical groove of the TkRadB filament is open and wide, not restricted by the additional N- or C-terminal domains as in the cases of other RecA/Rad51 filaments. Moreover, the pI of PfRadB is higher than that of PfRadA by 2.6 pH units, further augmenting its electrostatic binding to DNA. Likewise, the L1 and L2 loops in the axial regions are conveniently exposed for binding probably to ssDNA (Figure 6). These features would account for the higher DNA binding activity of PfRadB (10) than that of PfRadA.

From our view on the RadB–DNA interaction described above, RadB could be assumed as a non-specific scaffold for DNA. However, limited number of the molecules present in the cell (1/200 of the RadA molecules in *P.furiosus*) (10) suggests their localization at particular sites in the form of a monomer or a small oligomer rather than ubiquitous binding to DNA as a long filament. In the case of *P.furiosus*, RadB specifically interacts with Hjc, suppressing its Holliday junction cleavage activity in the absence of ATP but not with ATP (10). The *P.furiosus* Hjc protein resembles TkRadB in surface electrostatic properties: its calculated pI is rather high (10.0) and its calculated surface potentials is bipolar (46). The absence of ATP may favour a monomeric form of RadB, which might competitively inhibit Hjc from associating with a target DNA. An analogy could be drawn for the function of RadA since the specific interaction between PfRadA and PfRadB (10) is naturally inferred from the close structural similarity between TkRadB and the PfRadA core domain. In this respect, the filament of RadB seems to serve as a storage form.

Earlier observations on TkRadB have claimed a capability of the protein to complement RecA in *E.coli* (8) and a DNase activity (27,47), both of which are not observed in PfRadB; but they have been challenged by the recent report by Inwood *et al.* (28). These results were obtained from the experiment employing a mutant form of the protein, where the two C-terminal residues were replaced by 19 residues derived from the vector used; and these unusual functions seem to be ascribed to the extra sequence. Because the present structure has been obtained from the protein samples with the corrected sequence, we are unable to comment on these unusual but interesting artefacts.

## ACKNOWLEDGEMENTS

We thank Drs Naohiro Matsugaki, Noriyuki Igarashi, Mamoru Suzuki and Soichi Wakatsuki for their assistance with the data collection at the Photon Factory. Financial support from the New Energy and Industrial Technology Development Organization (NEDO) to K.H. is acknowledged. Funding to pay the Open Access publication charges for this article was provided by AIST.

*Conflict of interest statement.* None declared.

## REFERENCES

- Marguet,E. and Forterre,P. (1994) DNA stability at temperatures typical for hyperthermophiles. *Nucleic Acids Res.*, **22**, 1681–1686.
- Grogan,D.W. (2000) The question of DNA repair in hyperthermophilic archaea. *Trends Microbiol.*, **8**, 180–185.
- Peak,M.J., Robb,F.T. and Peak,J.G. (1995) Extreme resistance to thermally induced DNA backbone breaks in the hyperthermophilic archaeon *Pyrococcus furiosus*. *J. Bacteriol.*, **177**, 6316–6318.
- DiRuggiero,J., Santangelo,N., Nackerdien,Z., Ravel,J. and Robb,F.T. (1997) Repair of extensive ionizing-radiation DNA damage at 95°C in the hyperthermophilic archaeon *Pyrococcus furiosus*. *J. Bacteriol.*, **179**, 4643–4645.
- Aravind,L., Walker,D.R. and Koonin,E.V. (1999) Conserved domains in DNA repair proteins and evolution of repair systems. *Nucleic Acids Res.*, **27**, 1223–1242.
- Eisen,J.A. and Hanawalt,P.C. (1999) A phylogenomic study of DNA repair genes, proteins, and processes. *Mutat. Res.*, **435**, 171–213.
- Sandler,S.J., Satin,L.H., Samra,H.S. and Clark,A.J. (1996) *recA*-like genes from three archaean species with putative protein products similar to Rad51 and Dmc1 proteins of the yeast *Saccharomyces cerevisiae*. *Nucleic Acids Res.*, **24**, 2125–2132.
- Rashid,N., Morikawa,M. and Imanaka,T. (1996) A RecA/RAD51 homologue from a hyperthermophilic archaeon retains the major RecA domain only. *Mol. Gen. Genet.*, **253**, 397–400.
- DiRuggiero,J., Brown,J.R., Bogert,A.P. and Robb,F.T. (1999) DNA repair systems in archaea: mementos from the last universal common ancestor? *J. Mol. Evol.*, **49**, 474–484.
- Komori,K., Miyata,T., DiRuggiero,J., Holley-Shanks,R., Hayashi,I., Cann,I.K., Mayanagi,K., Shinagawa,H. and Ishino,Y. (2000) Both RadA and RadB are involved in homologous recombination in *Pyrococcus furiosus*. *J. Biol. Chem.*, **275**, 33782–33790.
- Reich,C.I., McNeil,L.K., Brace,J.L., Brucker,J.K. and Olsen,G.J. (2001) Archaeal RecA homologues: different response to DNA-damaging agents in mesophilic and thermophilic Archaea. *Extremophiles*, **5**, 265–275.
- Fernandez de Henestrosa,A.R., Calero,S. and Barbe,J. (1991) Expression of the *recA* gene of *Escherichia coli* in several species of gram-negative bacteria. *Mol. Gen. Genet.*, **226**, 503–506.
- Basile,G., Aker,M. and Mortimer,R.K. (1992) Nucleotide sequence and transcriptional regulation of the yeast recombinational repair gene RAD51. *Mol. Cell. Biol.*, **12**, 3235–3246.
- Hayashi,I., Morikawa,K. and Ishino,Y. (1999) Specific interaction between DNA polymerase II (PolD) and RadB, a Rad51/Dmc1 homologue, in *Pyrococcus furiosus*. *Nucleic Acids Res.*, **27**, 4695–4702.
- Egelman,E.H. and Stasiak,A. (1986) Structure of helical RecA–DNA complexes. Complexes formed in the presence of ATP- $\gamma$ -S or ATP. *J. Mol. Biol.*, **191**, 677–697.
- Yang,S., VanLoock,M.S., Yu,X. and Egelman,E.H. (2001) Comparison of bacteriophage T4 UvsX and human Rad51 filaments suggests that RecA-like polymers may have evolved independently. *J. Mol. Biol.*, **312**, 999–1009.
- Yang,S., Yu,X., Seitz,E.M., Kowalczykowski,S.C. and Egelman,E.H. (2001) Archaeal RadA protein binds DNA as both helical filaments and octameric rings. *J. Mol. Biol.*, **314**, 1077–1085.
- Yu,X., Jacobs,S.A., West,S.C., Ogawa,T. and Egelman,E.H. (2001) Domain structure and dynamics in the helical filaments formed by RecA and Rad51 on DNA. *Proc. Natl Acad. Sci. USA*, **98**, 8419–8424.
- Story,R.M., Weber,I.T. and Steitz,T.A. (1992) The structure of the *E. coli recA* protein monomer and polymer. *Nature*, **355**, 318–325.
- Datta,S., Prabu,M.M., Vaze,M.B., Ganesh,N., Chandra,N.R., Muniyappa,K. and Vijayan,M. (2000) Crystal structures of *Mycobacterium tuberculosis* RecA and its complex with ADP-AIF(4): implications for decreased ATPase activity and molecular aggregation. *Nucleic Acids Res.*, **28**, 4964–4973.
- Datta,S., Krishna,R., Ganesh,N., Chandra,N.R., Muniyappa,K. and Vijayan,M. (2003) Crystal structures of *Mycobacterium smegmatis* RecA and its nucleotide complexes. *J. Bacteriol.*, **185**, 4280–4284.
- Conway,A.B., Lynch,T.W., Zhang,Y., Fortin,G.S., Fung,C.W., Symington,L.S. and Rice,P.A. (2004) Crystal structure of a Rad51 filament. *Nature Struct. Mol. Biol.*, **11**, 791–796.
- Wu,Y., He,Y., Moya,I.A., Qian,X. and Luo,Y. (2004) Crystal structure of archaeal recombinase RadA: a snapshot of its extended conformation. *Mol. Cell*, **15**, 423–435.
- Shin,D.S., Pellegrini,L., Daniels,D.S., Yelent,B., Craig,L., Bates,D., Yu,D.S., Shivji,M.K., Hitomi,C., Arvai,A.S. *et al.* (2003) Full-length archaeal Rad51 structure and mutants: mechanisms for RAD51 assembly and control by BRCA2. *EMBO J.*, **22**, 4566–4576.
- Kinebuchi,T., Kagawa,W., Enomoto,R., Tanaka,K., Miyagawa,K., Shibata,T., Kurumizaka,H. and Yokoyama,S. (2004) Structural basis for octameric ring formation and DNA interaction of the human homologous-pairing protein Dmc1. *Mol. Cell*, **14**, 363–374.
- Harata,K., Ishii,N., Rashid,N., Morikawa,M. and Imanaka,T. (2000) Crystallization and preliminary X-ray study of Pk-REC from a hyperthermophilic archaeon, *Pyrococcus kodakaraensis* KOD1. *Acta Crystallogr.*, **D56**, 648–649.
- Rashid,N., Morikawa,M., Kanaya,S., Atomi,H. and Imanaka,T. (1999) A unique DNase activity shares the active site with ATPase activity of the RecA/Rad51 homologue (Pk-REC) from a hyperthermophilic archaeon. *FEBS Lett.*, **445**, 111–114.
- Inwood,W., Kane,S., DiRuggiero,J., Robb,F. and Clark,A.J. (2001) The RadB protein from *Pyrococcus* does not complement *E. coli recA* mutations *in vivo*. *Mol. Genet. Genomics*, **265**, 683–686.

29. La Fortelle, E.d. and Bricogne, G. (1997) Maximum-likelihood heavy-atom parameter refinement in the MIR and MAD methods. *Methods Enzymol.*, **276**, 472–494.
30. Collaborative Computational Project, Number 4 (1994), The CCP4 suite: programs for protein crystallography. *Acta Crystallogr.*, **D50**, 760–763.
31. Roussel, A. and Cambillau, C. (1991) TURBO-FRODO: A Tool for Building Structural Models. In Silicon Graphics (ed.), *Silicon Graphics Geometry Partners Directory*. Silicon Graphics, Mountain View, CA, pp. 86.
32. Brünger, A.T. (1992) X-PLOR version 3.1: a system for X-ray crystallography and NMR. Yale University Press, New Haven.
33. Otwinowski, Z. and Minor, W. (1997) Processing of X-ray diffraction data collected in oscillation mode. *Methods Enzymol.*, **276**, 307–326.
34. Brünger, A.T., Adams, P.D., Clore, G.M., DeLano, W.L., Gros, P., Grosse-Kunstleve, R.W., Jiang, J.S., Kuszewski, J., Nilges, M., Pannu, N.S. *et al.* (1998) Crystallography and NMR system: a new software suite for macromolecular structure determination. *Acta Crystallogr.*, **D54**, 905–921.
35. Lu, G. (2000) TOP: a new method for protein structure comparisons and similarity searches. *J. Appl. Crystallogr.*, **33**, 176–183.
36. Kabsch, W. (1976) A solution for the best rotation to relate two sets of vectors. *Acta Crystallogr.*, **A32**, 922–923.
37. Kraulis, P.J. (1991) Molscript—a program to produce both detailed and schematic plots of protein structures. *J. Appl. Crystallogr.*, **24**, 946–950.
38. Nicholls, A. and Honig, B. (1991) A rapid finite-difference algorithm, utilizing successive over-relaxation to solve the Poisson–Boltzmann equation. *J. Comput. Chem.*, **12**, 435–445.
39. Pellegrini, L., Yu, D.S., Lo, T., Anand, S., Lee, M., Blundell, T.L. and Venkitaraman, A.R. (2002) Insights into DNA recombination from the structure of a RAD51–BRCA2 complex. *Nature*, **420**, 287–293.
40. Walker, J.E., Saraste, M., Runswick, M.J. and Gay, N.J. (1982) Distantly related sequences in the  $\alpha$ - and  $\beta$ -subunits of ATP synthase, myosin, kinases and other ATP-requiring enzymes and a common nucleotide binding fold. *EMBO J.*, **1**, 945–951.
41. Xing, X. and Bell, C.E. (2004) Crystal structures of *Escherichia coli* RecA in a compressed helical filament. *J. Mol. Biol.*, **342**, 1471–1485.
42. Rajan, R. and Bell, C.E. (2004) Crystal structure of RecA from *Deinococcus radiodurans*: insights into the structural basis of extreme radioresistance. *J. Mol. Biol.*, **344**, 951–963.
43. Lauder, S.D. and Kowalczykowski, S.C. (1991) Asymmetry in the recA protein–DNA filament. *J. Biol. Chem.*, **266**, 5450–5458.
44. Komori, K., Miyata, T., Daiyasu, H., Toh, H., Shinagawa, H. and Ishino, Y. (2000) Domain analysis of an archaeal RadA protein for the strand exchange activity. *J. Biol. Chem.*, **275**, 33791–33797.
45. Mikawa, T., Masui, R., Ogawa, T., Ogawa, H. and Kuramitsu, S. (1995) N-terminal 33 amino acid residues of *Escherichia coli* RecA protein contribute to its self-assembly. *J. Mol. Biol.*, **250**, 471–483.
46. Nishino, T., Komori, K., Tsuchiya, D., Ishino, Y. and Morikawa, K. (2001) Crystal structure of the archaeal holliday junction resolvase Hjc and implications for DNA recognition. *Structure*, **9**, 197–204.
47. Rashid, N., Morikawa, M., Nagahisa, K., Kanaya, S. and Imanaka, T. (1997) Characterization of a RecA/RAD51 homologue from the hyperthermophilic archaeon *Pyrococcus* sp. KOD1. *Nucleic Acids Res.*, **25**, 719–726.